Transit Met Chem (2016) 41:879–887
DOI 10.1007/s11243-016-0090-z

# Modification of the structure and magnetic properties of fumarato-bridged Mn coordination polymers through different dimethyl-2,2′-bipyridine co-ligands

**Antonio Téllez-López[1] · Víctor Sánchez-Mendieta[1,2] · Jonathan Jaramillo-García[1] · Luis D. Rosales-Vázquez[1] · Iván García-Orozco[2] · Raúl A. Morales-Luckie[2] · Roberto Escudero[3] · Francisco Morales-Leal[3]**

Received: 8 June 2016 / Accepted: 22 August 2016 / Published online: 2 September 2016


**Abstract** Manganese coordination polymers $\{Mn(fum)(5dmb)(H_2O)_2\}_n$ (**1**) and $\{[Mn_2(fum)_2(4dmb)_2]\cdot H_2O\}_n$ (**2**) (fum = fumarato; 5dmb = 5,5′-dimethyl-2,2′-bipyridine; 4dmb = 4,4′-dimethyl-2,2′-bipyridine) were obtained from one-pot, solution reactions under ambient conditions. The fum ligand acquires different coordination modes in the presence of the different dmb ancillary ligands, promoting distinctive crystal structures, including divergent dimensionalities. Thus, X-ray single-crystal data reveal that complex **1** crystallizes in a monoclinic system with C2/c space group and forms an infinite one-dimensional polymer. The Mn(II) center is six-coordinated and displays a distorted octahedral configuration. In addition, the solid-state self-assembly of the polymeric structure of **1** gives rise to a two-dimensional (2D) supramolecular framework, mainly through hydrogen bonding. In contrast, complex **2** crystallizes in a monoclinic system with a Cc space group and forms an infinite 2D coordination polymer having dinuclear units. The Mn(II) center has a distorted octahedral configuration. The thermal stabilities of both coordination polymers were investigated. Variable-temperature magnetic measurements show that complex **1** is paramagnetic, while complex **2** exhibits weak antiferromagnetic coupling between adjacent Mn(II) centers.

**Electronic supplementary material** The online version of this article (doi:10.1007/s11243-016-0090-z) contains supplementary material, which is available to authorized users.

✉ Víctor Sánchez-Mendieta
vsanchezm@uaemex.mx

✉ Roberto Escudero
escu@unam.mx

[1] Facultad de Química, Universidad Autónoma del Estado de México, Paseo Colón y Paseo Tollocan, Toluca, Estado de México 50120, Mexico

[2] Centro Conjunto de Investigación en Química Sustentable UAEM-UNAM, Carretera Toluca-Ixtlahuaca Km. 14.5, Tlachaloya, Toluca, Estado de México, Mexico

[3] Instituto de Investigaciones en Materiales, Universidad Nacional Autónoma de México, Apartado Postal 70-360, Mexico, Distrito Federal 04510, Mexico

## Introduction

Research into the fundamental properties of coordination polymers continues to be relevant, due to the synergic relationship between structural and physicochemical characteristics. In particular, the search for tailor-made synthetic methodologies capable of producing desired properties for applications of these materials has long been pursued [1]. Several strategies have been developed to synthesize mixed ligand coordination polymers of bivalent transition metals containing nitrogen and oxygen donor ligands [2]. Self-assembly of small molecules, compounds or complexes has proved to be a valuable procedure for the synthesis of large structures with a minimum of effort. However, the self-assembly process is sometimes accompanied by an uncertainty halo, due to unpredictable interactions among metal centers and ligands, especially when weak forces (e.g., hydrogen bonding, $\pi$–$\pi$ interactions) and/or solvents, such as water, are involved [3]. Crystal engineering refers to the construction of crystal structures from organic and metal–organic compounds using design principles that come from an understanding of the intermolecular interactions in the molecular solids [4]. Also, supramolecular frameworks based on metal centers and organic ligands have gained interest recently, due to their

fascinating structural diversity and their potential applications in catalysis, sensing, porosity and nonlinear optics [5]. Among the most used bridging ligands for transition metals are the dicarboxylates [6]. In particular, the fumarato (fum) ligand has been extensively used for the formation of complexes [7] and coordination polymers [8]. We selected this ionic bridging ligand due to its simple chemical structure and its dual chemical functionality, which allows for the generation of complexes or polymers, depending on its coordination modes. The use of 2,2′-bipyridine as an ancillary ligand had become relevant in our previous studies on complexes [9] and coordination polymers [10] of transition metals. Previous reports deal mainly with structural studies of coordination polymers formed by the reaction of Mn(II) salts with fum as a bridging ligand and 2,2′-bipyridine [11], and the related 1,10-phenanthroline [12], as co-ligands. Magnetism studies were, however, not reported for those compounds. Thus, we decided to continue with one of the most studied nitrogen donor ligands [13], but varying its alkyl substituent, in order to verify the influence of steric properties of the co-ligand on the dimensionalities and crystalline structures of the resulting coordination polymers. So far, very few articles have been published on the use of different di-alkyl-2,2′-bipyridines as ancillary ligands, either in transition metal complexes [14] or coordination polymers [15, 16], and none of them have focused on the influence of steric effects on the structures and, consequently, their properties.

Herein, we describe the synthesis, crystalline molecular and supramolecular structures, thermal analyses and magnetic properties of two coordination polymers of Mn(II), **1** and **2**, bearing fum as a bridging ligand and two different dimethyl-2,2′-bipyridines as ancillary ligands.

## Experimental

All chemicals were of analytical grade, purchased commercially (Aldrich) and used without further purification. All syntheses were carried out under aerobic and ambient conditions. Elemental analyses for C, H and N were obtained by standard methods using a Vario Micro-Cube analyzer. IR spectra of the complexes were determined as KBr disks on an Avatar 360 FT-IR Nicolet spectrophotometer from 4000 to 400 $cm^{-1}$. Thermogravimetric analyses were performed on a TA Instruments analyzer, under $N_2$ atmosphere, at a heating rate of 10 °C $min^{-1}$, from 20 to 800 °C. Magnetic characteristics of the complexes were determined with a MPMS Quantum Design magnetometer, with measurements performed at zero-field cooling (ZFC) and field cooling (FC) from 2 to 300 K and decreasing. The applied magnetic field was 100 Oe, and diamagnetic corrections were estimated using Pascal's constants as $-250 \times 10^{-6}$ $cm^3$ $mol^{-1}$.

### Synthesis of $\{Mn(fum)(5dmb)(H_2O)_2\}_n$ (1)

A solution of 5,5′-dimethyl-2,2′-bipyridine (0.0921 g; 0.5 mmol) in methanol (60 ml) was added to an aqueous solution (30 ml) of sodium fumarate (0.0800 g; 0.5 mmol), while stirring. A solution of $MnCl_2{\cdot}4H_2O$ (0.0989 g; 0.5 mmol) in de-ionized water (30 ml) was added. A translucent yellow solution was obtained. After 4 days, small yellow crystals were obtained; these were filtered out, washed with a 50:50 deionized water–methanol mixture and air-dried. Yield: 76 % based on metal precursor. Anal. calc. for $C_{16}H_{18}MnN_2O_6$ (FW = 389.16): C, 49.35; H, 4.62; N, 7.19 %. Found: C, 48.91; H, 4.60; N, 7.09 %. IR ($cm^{-1}$): 3225 (vs, br), 2910 (s), 1960 (w), 1900 (w), 1830 (w), 1701 (w), 1545 (s), 1480 (s, sh), 1365 (s), 1242 (m), 1200 (m), 1160 (m), 1040 (m), 1003 (w), 730 (w), 675 (s, sh), 580 (s, sh), 470 (m), 413 (m).

### Synthesis of $\{[Mn_2(fum)_2(4dmb)_2]{\cdot}H_2O\}_n$ (2)

A solution of fumaric acid (0.0348 g; 0.3 mmol) in methanol (5 ml) was added to an aqueous solution (5 ml) of sodium hydroxide (0.0240 g; 0.6 mmol), while stirring. Then, a solution of $MnCl_2{\cdot}4H_2O$ (0.0593 g; 0.3 mmol) in deionized water (5 ml) was added, under constant stirring. Finally, a solution of 4,4′-dimethyl-2,2′-bipyridine (0.0552 g; 0.3 mmol) in methanol (5 ml) was added. A translucent yellow solution was obtained. After six days, the yellow crystals so obtained were filtered out, washed with a 50:50 deionized water–methanol mixture and air-dried. Yield: 42 % based on metal precursor. Anal. calc. for $C_{32}H_{34}Mn_2N_4O_{11}$ (FW = 724.48): C, 53.05; H, 4.17; N, 7.73 %. Found: C, 52.86; H, 4.29; N, 7.68 %. IR ($cm^{-1}$): 3630 (s), 3500 (s, br), 3080 (m), 3060(s), 2960 (m), 2920 (m), 1960 (m), 1940 (m), 1880 (w), 1820 (w), 1600 (vs), 1550 (vs), 1480 (s), 1390 (s), 1300 (m), 1240 (m), 1210 (m), 1130 (w), 1010 (s), 980 (m), 918 (s), 833 (s), 802 (s), 706 (m), 690 (vs, sh), 660 (s), 586 (s), 548 (m), 513 (m), 424 (w).

#### *Crystal structure determination and refinement*

Crystallographic data for both complexes were collected on a Bruker SMART APEX DUO three-circle diffractometer equipped with an Apex II CCD detector using MoKα radiation ($\lambda = 0.71073$ Å, Incoatec IμS microsource) at 100 K [17]. The crystals were coated with hydrocarbon oil, picked up with a nylon loop and immediately mounted in the cold nitrogen stream (100 K) of the diffractometer. The structures were solved by direct methods (SHELXS-97)

and refined by full-matrix least-squares on $F^2$ [18] using the shelXle GUI [19]. The hydrogen atoms of the C–H bonds were placed in idealized positions. The hydrogen atoms from $H_2O$ moieties were localized from the difference electron density map, and their positions were refined with $U_{iso}$ tied to the parent atom with distance restraints. The water molecule of crystallization in **2** was disordered over two sets of positions. The disordered hydrogens were refined using distance restraints (DFIX). The crystallographic data and refinement details for both polymers are summarized in Table 1. Selected bond lengths and angles for **1** and **2** are listed in Tables 2 and 3, respectively.

## Results and discussion

### Synthesis and structures

Using a very simple methodology of self-assembling solution reactions, equivalent amounts of sodium fumarate, $MnCl_2$ and 5,5′-dimethyl-2,2′-bipyridine (5dmb) or 4,4′-dimethyl-2,2′-bipyridine (4dmb) were mixed in water–methanol solutions under ambient conditions. Slow evaporation of solvents yielded light yellow crystals of complexes **1** and **2**. These crystals are insoluble in common solvents and appear to be air and moisture stable.

The IR spectra of both complexes show the typical bands (vide supra) expected for carboxylate ligands coordinated to Mn(II) (11, 12). The main variances may come from the different coordination modes acquired by the fum ligands in these complexes. In **1**, the asymmetric carboxylate stretch occurs at 1545 $cm^{-1}$ along with the symmetric stretch at 1480 $cm^{-1}$, and the separation of the two bands is as expected for the monodentate coordination form. The IR spectrum of complex **2** shows two sets of asymmetric stretches for the carboxylate moiety at 1660 and 1550 $cm^{-1}$, with the corresponding symmetric stretches at 1480 and 1390 $cm^{-1}$. The differences between asymmetric and symmetric stretch for the carboxylate ion ($\Delta\nu_{COO}^{-}$) are 180 and 160 $cm^{-1}$, respectively. These bands

**Table 1** Crystal data and structure refinement parameters for **1** and **2**

| | **1** | **2** |
|---|---|---|
| Empirical formula | $C_{16}H_{18}MnN_2O_6$ | $C_{32}H_{30}Mn_2N_4O_9$ |
| Formula weight | 389.26 | 724.48 |
| Temperature (K) | 100(2) | |
| Wavelength (Å) | 0.71073 | |
| Crystal system | Monoclinic | Monoclinic |
| Space group | C2/c | Cc |
| *a* (Å) | 7.0116(2) | 7.8917(3) |
| *b* (Å) | 17.3753(4) | 20.1889(7) |
| *c* (Å) | 13.7100(3) | 19.8231(7) |
| α (°) | 90 | 90 |
| β (°) | 97.8556(5) | 98.1991(6) |
| γ (°) | 90 | 90 |
| Volume ($Å^3$) | 1654.60(7) | 3126.0(2) |
| *Z* | 4 | 4 |
| $D_{calc}$ ($Mg/m^3$) | 1.563 | 1.539 |
| Absorption coefficient ($mm^{-1}$) | 0.834 | 0.870 |
| *F*(000) | 804 | 1488 |
| Crystal size ($mm^3$) | 0.216 × 0.203 × 0.168 | 0.349 × 0.193 × 0.162 |
| Theta range for data collection (°) | 2.344–26.021 | 2.017–25.349 |
| Index ranges | $-8 \le h \le 8$, $21 \le k \le 21$, $-16 \le l \le 16$ | $-9 \le h \le 9$, $-24 \le k \le 24$, $-23 \le l \le 23$ |
| Reflections collected | 11,994 | 28,301 |
| Independent reflections | 1623 [$R$(int) = 0.0235] | 5730 [$R$(int) = 0.0200] |
| Refinement method | Full-matrix least-squares on $F^2$ | |
| Data/restraints/parameters | 1623/94/158 | 5730/23/453 |
| Goodness-of-fit on $F^2$ | 1.068 | 1.065 |
| Final $R$ indices [$I > 2$sigma(I)] | $R1 = 0.0197$, w$R2 = 0.0509$ | $R1 = 0.0216$, w$R2 = 0.0609$ |
| $R$ indices (all data) | $R1 = 0.0202$, w$R2 = 0.0513$ | $R1 = 0.0218$, w$R2 = 0.0610$ |
| Largest diff. peak and hole e ($Å^{-3}$) | 0.292 and −0.235 | 0.458 and −0.202 |

**Table 2** Selected bond distances (Å) and angles (°) for **1**

| | | | |
|---|---|---|---|
| Bond lengths (Å) | | | |
| Mn(1)–O(1)#1 | 2.161(5) | Mn(1)–O(3)#1 | 2.1665(9) |
| Mn(1)–O(1) | 2.161(5) | Mn(1)–N(1) | 2.2818(10) |
| Mn(1)–O(1A) | 2.163(5) | Mn(1)–N(1)#1 | 2.2818(10) |
| Mn(1)–O(1A)#1 | 2.163(5) | | |
| Mn(1)–O(3) | 2.1665(9) | | |
| Angles (°) | | | |
| O(1)#1–Mn(1)–O(1) | 163.2(10) | O(1)–Mn(1)–N(1) | 103.4(4) |
| O(1A)–Mn(1)–O(1A)#1 | 167.0(10) | O(1A)–Mn(1)–N(1) | 98.3(4) |
| O(1)#1–Mn(1)–O(3) | 85.8(5) | O(1A)#1–Mn(1)–N(1) | 92.2(5) |
| O(1)–Mn(1)–O(3) | 83.5(3) | O(3)–Mn(1)–N(1) | 164.20(4) |
| O(1A)–Mn(1)–O(3) | 89.3(4) | O(3)#1–Mn(1)–N(1) | 94.05(4) |
| O(1A)#1–Mn(1)–O(3) | 82.4(5) | O(1)#1–Mn(1)–N(1)#1 | 103.4(4) |
| O(1)#1–Mn(1)–O(3)#1 | 83.5(3) | O(1)–Mn(1)–N(1)#1 | 90.3(5) |
| O(1)–Mn(1)–O(3)#1 | 85.8(5) | O(1A)–Mn(1)–N(1)#1 | 92.2(5) |
| O(1A)–Mn(1)–O(3)#1 | 82.4(5) | O(1A)#1–Mn(1)–N(1)#1 | 98.3(4) |
| O(1A)#1–Mn(1)–O(3)#1 | 89.3(4) | O(3)–Mn(1)–N(1)#1 | 94.05(4) |
| O(3)–Mn(1)–O(3)#1 | 100.69(5) | O(3)#1–Mn(1)–N(1)#1 | 164.20(4) |
| O(1)#1–Mn(1)–N(1) | 90.3(5) | N(1)–Mn(1)–N(1)#1 | 71.97(5) |

| D–H…A | *d*(D–H) | *d*(H…A) | *d*(D…A) | <(DHA) |
|---|---|---|---|---|
| O(3)–H(3A)…O(2A) | 0.852(13) | 2.018(9) | 2.7158(19) | 138.6(16) |
| O(3)–H(3A)…O(2A)#3 | 0.852(13) | 1.845(16) | 2.6536(19) | 158.0(15) |
| O(3)–H(3B)…O(2)#1 | 0.811(15) | 2.106(19) | 2.7275(19) | 133(2) |
| O(3)–H(3B)…O(2)#4 | 0.811(15) | 1.902(16) | 2.6879(19) | 163(2) |

Symmetry transformations used to generate equivalent atoms

#1: $-x + 1, y, -z + 3/2$; #2: $-x, -y + 1, -z + 1$; #3: $-x, y, -z + 3/2$; #4: $x, -y + 1, z + 1/2$

can be assigned to the bidentate chelate and bidentate bridging coordination modes of the fum ligand in **2**. $\{Mn(fum)(5dmb)(H_2O)_2\}_n$ (**1**) crystallizes in a monoclinic system with C2/c space group and forms an infinite one-dimensional (1D) coordination polymer (Fig. 1). The repeat molecular unit contains one Mn center, one fum ligand, one 5dmb co-ligand and two coordinated water ligands. The coordination environment of the Mn is shown in Fig. 1a; the metal is six-coordinated and surrounded by four oxygen atoms from two different fum ligands and the two water ligands, plus two nitrogen atoms from one 5dmb ligand. The Mn has a distorted octahedral configuration. The Mn–O bond lengths range from 2.161(5) to 2.1665(9) Å, while the Mn–N distance is 2.2818(10) Å, these values are comparable to those found on similar Mn(II) compounds [20–22]. In complex **1**, a 1D zig-zag chain is formed due to the monodentate $\eta^1{:}\eta^0$ coordination mode of fum, together with the *trans* configuration of its carboxylate groups, thus bridging the Mn ions (Fig. 1b). The Mn···Mn distance in the 1D chain is 9.885 Å.

Intermolecular hydrogen-bonding interactions assemble complex **1** into a 2D supramolecular array (Fig. 2). These interactions are promoted by the presence of the aqua ligand and the non-coordinated oxygen atom of the fum carboxylate. This is shown in Fig. 2, where the main O–H···O interactions involve the O–H moiety (O3) of the aqua ligand with each oxygen atom (O2) of the non-coordinated side of one fum ligand, in an intramolecular hydrogen bond. Furthermore, each water ligand generates a double hydrogen bridge; the one described above and another with one fum oxygen atom (O3) coordinated to Mn(II) of a neighboring 1D polymeric chain (intermolecular hydrogen bonding). In this way, an extended 2D supramolecular array is generated (Fig. 2 and Fig. S1, supplementary data), in which the intermolecular shortest Mn···Mn distance is 7.012 Å. In addition, the crystalline lattice of **1** includes interchain $\pi$–$\pi$ stacking interactions from the pyridine rings of the 5dmb ligand, with distances of 3.999 and 4.860 Å.

$\{[Mn_2(fum)_2(4dmb)_2]\cdot H_2O\}_n$ (**2**) crystallizes in a monoclinic system with Cc space group and forms an infinite two-dimensional (2D) coordination polymer. The molecular structure of **2** consists of two crystallographic independent $Mn^{2+}$ centers, two fum ligands, two 4dmb ligands and one guest $H_2O$ molecule (Fig. 3). Both Mn atoms are six-

**Table 3** Selected bond distances (Å) and angles (°) for **2**

| | | | |
|---|---|---|---|
| Bond lengths (Å) | | | |
| Mn(1)–O(4)#1 | 2.111(2) | Mn(2)–O(2)#3 | 2.084(2) |
| Mn(1)–O(1) | 2.111(2) | Mn(2)–O(3) | 2.106(2) |
| Mn(1)–O(7)#2 | 2.232(2) | Mn(2)–O(5) | 2.236(2) |
| Mn(1)–N(2) | 2.253(3) | Mn(2)–N(3) | 2.240(3) |
| Mn(1)–N(1) | 2.264(3) | Mn(2)–N(4) | 2.265(3) |
| Mn(1)–O(8)#2 | 2.315(2) | Mn(2)–O(6) | 2.317(2) |
| Mn(1)–C(33)#2 | 2.599(3) | Mn(2)–C(29) | 2.607(3) |
| Angles (°) | | | |
| O(4)#1–Mn(1)–O(1) | 99.90(9) | O(2)#3–Mn(2)–O(5) | 102.25(9) |
| O(4)#1–Mn(1)–O(7)#2 | 94.81(9) | O(3)–Mn(2)–O(5) | 97.65(9) |
| O(1)–Mn(1)–O(7)#2 | 94.49(8) | O(2)#3–Mn(2)–N(3) | 88.57(9) |
| O(4)#1–Mn(1)–N(2) | 170.45(10) | O(3)–Mn(2)–N(3) | 104.90(9) |
| O(1)–Mn(1)–N(2) | 86.75(9) | O(5)–Mn(2)–N(3) | 152.11(9) |
| O(7)#2–Mn(1)–N(2) | 91.47(9) | O(2)#3–Mn(2)–N(4) | 160.35(10) |
| O(4)#1–Mn(1)–N(1) | 99.11(9) | O(3)–Mn(2)–N(4) | 85.85(9) |
| O(1)–Mn(1)–N(1) | 107.86(9) | O(5)–Mn(2)–N(4) | 93.71(9) |
| O(7)#2–Mn(1)–N(1) | 151.03(9) | N(3)–Mn(2)–N(4) | 72.11(9) |
| N(2)–Mn(1)–N(1) | 72.17(9) | O(2)#3–Mn(2)–O(6) | 93.66(9) |
| O(4)#1–Mn(1)–O(8)#2 | 90.29(8) | O(3)–Mn(2)–O(6) | 153.31(8) |
| O(1)–Mn(1)–O(8)#2 | 151.69(8) | O(5)–Mn(2)–O(6) | 58.06(8) |
| O(7)#2–Mn(1)–O(8)#2 | 58.14(8) | N(3)–Mn(2)–O(6) | 96.05(9) |
| N(2)–Mn(1)–O(8)#2 | 86.91(9) | N(4)–Mn(2)–O(6) | 85.04(9) |
| N(1)–Mn(1)–O(8)#2 | 96.34(9) | O(2)#3–Mn(2)–C(29) | 99.91(9) |
| O(4)#1–Mn(1)–C(33)#2 | 93.08(9) | O(3)–Mn(2)–C(29) | 126.00(9) |
| O(1)–Mn(1)–C(33)#2 | 123.34(9) | O(5)–Mn(2)–C(29) | 29.34(9) |
| O(7)#2–Mn(1)–C(33)#2 | 29.18(9) | N(3)–Mn(2)–C(29) | 123.95(10) |
| N(2)–Mn(1)–C(33)#2 | 88.88(9) | N(4)–Mn(2)–C(29) | 88.37(9) |
| N(1)–Mn(1)–C(33)#2 | 124.15(9) | O(6)–Mn(2)–C(29) | 28.75(9) |
| O(8)#2–Mn(1)–C(33)#2 | 28.96(9) | | |
| O(2)#3–Mn(2)–O(3) | 103.07(9) | | |

| D–H…A | *d*(D–H) | *d*(H…A) | *d*(D…A) | <(DHA) |
|---|---|---|---|---|
| O(9)–H(9A)…O(5) | 0.828(14) | 2.21(2) | 3.027(5) | 167(5) |
| O(9)–H(9B)…O(4) | 0.831(16) | 2.49(2) | 3.271(5) | 158(5) |
| O(9A)–H(9C)…O(5) | 0.891(19) | 2.03(3) | 2.857(10) | 153(6) |
| O(9B)–H(9E)…O(4) | 0.96(3) | 2.03(3) | 2.878(10) | 147(4) |

Symmetry transformations used to generate equivalent atoms

#1: $x + 1, y, z$; #2: $x + 2, -y + 1, z + ½$; #3: $x - 1, y, z$; #4: $x - 2, -y + 1, z - 1/2$

coordinated, being surrounded by four oxygen atoms from three different fum ligands and two nitrogen atoms from one 4dmb co-ligand in a distorted octahedral configuration. The Mn–O bond lengths vary from 2.084(2) to 2.315(2) Å, while the Mn–N distances range from 2.240(3) to 2.265(3) Å, comparable values to those found in related Mn(II) complexes [16, 23–25]. The fum ligand assumes a $\mu_4$ coordination mode, in which two carboxylate groups show $\mu_2$–$\eta^1$:$\eta^1$ bidentate coordination. The carboxylate moieties of the fum ligands alternately bridge adjacent Mn(II) centers in a *syn–syn* configuration, generating dinuclear units in a 1D chain motif. In these units, the Mn···Mn shortest separation is 4.561 Å. These dinuclear units are further linked by another fum ligand in a bridging $\eta^1$:$\eta^1$ bidentate fashion, giving double-ion rows (Fig. S2, supplementary data). These two different coordination modes of the fum ligands give rise to a distinctive 2D wrinkle-sheet array (Fig. S3, supplementary data). The crystalline lattice of **2** also shows interlayer $\pi$–$\pi$ stacking interactions from the pyridine rings of the 4dmb ligands, with distances

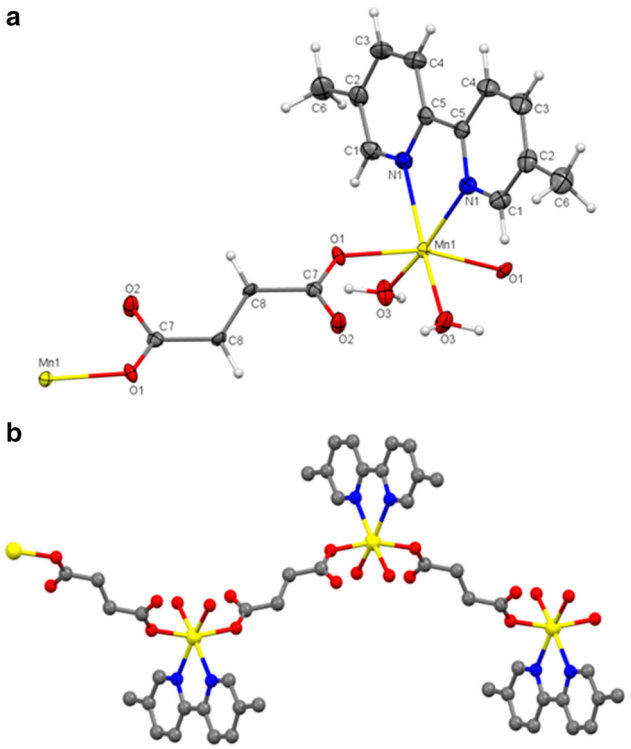


**Fig. 1** Molecular structure of $\{Mn(fum)(5dmb)(H_2O)_2\}_n$ (**1**) (ellipsoids shown at 60 % probability) (**a**); 1D zig-zag polymer chain of **1**, looking almost down *c* axis; hydrogens omitted for clarity (**b**)

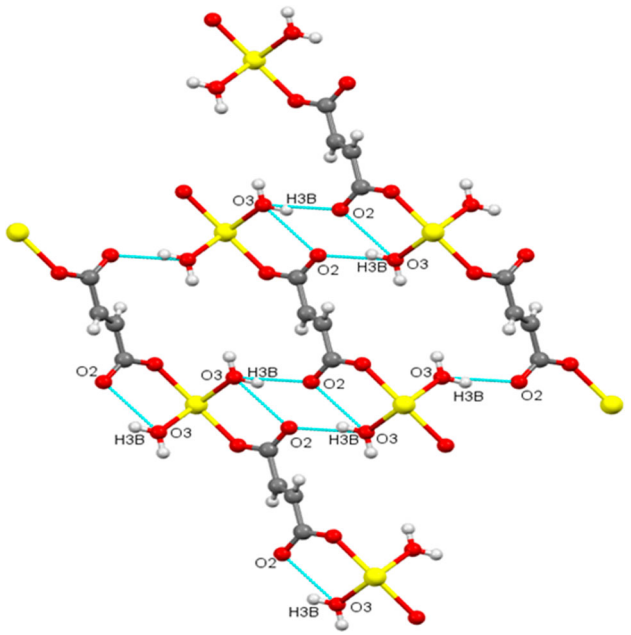


**Fig. 2** Hydrogen bonding main connections in **1**, view looking down *b* axis; 5dmb ligand is omitted for clarity

ranging from 3.649 to 5.803 Å. A water molecule of crystallization in the unit cell occupies three different positions, very near to each other. This disordered water molecule has hydrogen bonding interactions with the oxygen atoms (O4 and O5) of the coordinated carboxylates.

The three diverse coordination modes of the fum ligands, specifically $\eta^1{:}\eta^0$, $\eta^1{:}\eta^1$ and $\mu_2{-}\eta^1{:}\eta^1$, occurring in polymers **1** and **2**, respectively, seem to be promoted by the different dmb co-ligands in the two complexes. In complex **1**, the steric hindrance of the 5dmb ancillary ligand probably precludes further coordination of the oxygen atoms from the fum ligand to additional Mn centers, resulting in a 1D polymer, which by the virtue of a water ligand, is assembled into a stable 2D supramolecular structure by hydrogen bonds. In complex **2,** the 4dmb co-ligand has a less hindered structure, allowing the fum carboxylates to coordinate further with Mn. Interestingly, the coordination spheres and supramolecular structures of **1** and **2** contrast with those previously obtained for similar polymers assembled from fum and 2,2′-bipyridine (bipy) as co-ligands. Devereux et al. [12] obtained a 1D polymer in which the fum ligands connect seven coordinate Mn(II) centers, which are bonded to a bipy, two bidentate carboxylates and one aqua ligand, generating the polymer $\{Mn(fum)(bipy)(H_2O)\}_n$. Similar to **1**, this polymer has also a 2D supramolecular array due to hydrogen bonds. The lower coordination numbers obtained for **1** and **2**, where dimethyl-2,2′-bipyridines have been employed, compared to $\{Mn(fum)(bipy)(H_2O)\}_n$, indicate that in such coordination polymers the steric hindrance of the alkyl group influences the coordination sphere of the metal, and consequently, the structural dimensionality of the polymer.

## Thermogravimetric analyses

To examine the thermal stabilities of the crystalline polymers, thermal analyses were performed for complexes **1** and **2** between 20 and 800 °C (Fig. 4). Both complexes show three main stages of decomposition. The first major weight loss (10.0 %) for **1** occurs between 120 and 160 °C; the second, with a weight loss of 46.0 % of the initial weight, takes place approximately between 258 and 325 °C. The final weight loss (20.3 %) occurs around 390–430 °C, after which only 18 % of the initial sample weight remains at 800 °C. Similarly, for complex **2**, the first weight loss (∼2.6 %) appears between 97 and 252 °C, and the second, with a weight loss of 48.4 %, occurs between 275 and 386 °C. The final loss (∼20 %) occurs from 390 to 445 °C, leaving around 27 % of the initial sample weight at 800 °C. In both complexes, the first decomposition stage can be ascribed to the loss of water; however, for complex **1,** two coordinated water ligands are lost, while for complex **2,** only one crystallization water molecule is lost. The other stages can be attributed to the combined weight loss of the fum ligand (calcd. 29.3 % for **1** and 31.5 % for **2**), and the 5dbpy (calcd. 47.3 %) and the

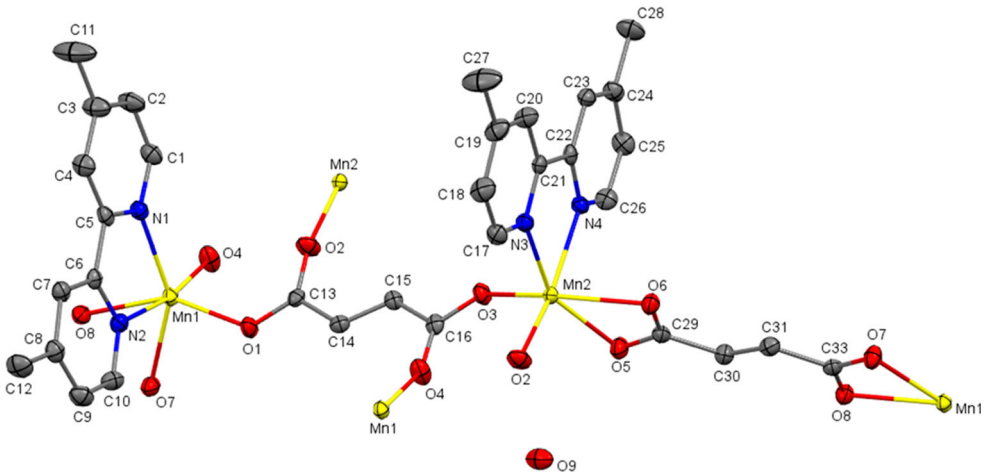


**Fig. 3** Molecular structure of $\{[Mn_2(fum)_2(4dmb)_2]\cdot H_2O\}_n$ (**2**) (ellipsoids shown at 60 % probability)

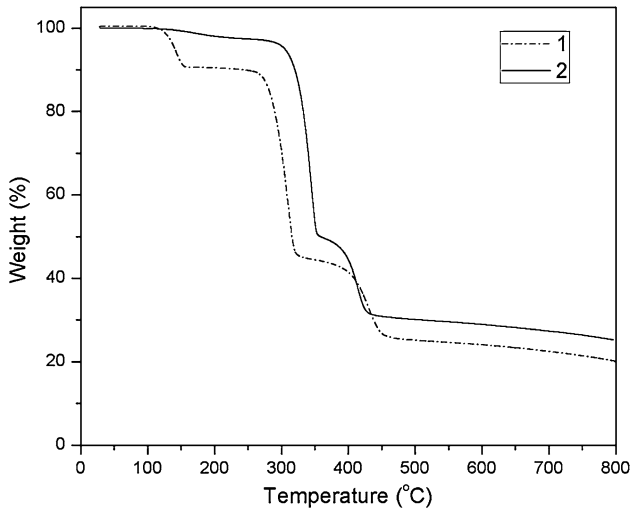


**Fig. 4** TGA plots for polymers **1** and **2**

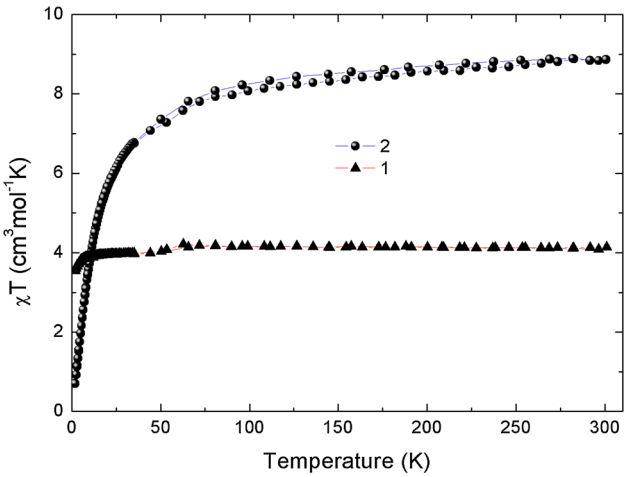


**Fig. 5** $\chi T$ versus $T$ plots for **1** and **2**

4dmb (calcd. 50.9 %) co-ligands, respectively. The residual material, at 800 °C, for both complexes, approximates to residual MnO (calcd. 18.2 % for **1** and 19.6 % for **2**). It is evident that due to their different structural characteristics, polymer **2** has superior thermal stability compared to **1** (Fig. 4).

## Magnetic properties

DC magnetic susceptibility, $\chi$, was determined for the complexes at zero-field cooling (ZFC) and field cooling (FC) modes, from 2–300 K and decreasing, in an applied field of 1000 Oe. The values of $\chi T$ at room temperature are 4.14 and 8.85 $cm^3\ mol^{-1}$ K for **1** and **2**, respectively, which are close to those expected for one (4.37 $cm^3\ mol^{-1}$ K) and two (8.75 $cm^3\ mol^{-1}$ K) magnetically isolated $Mn^{2+}$ ($S = 5/2$). However, on lowering the temperature, the $\chi T$ value of complex **1** remains almost constant (Fig. 5) and is only slightly diminished at very low temperature, showing that this compound behaves as a paramagnetic system. In contrast to this behavior, the $\chi T$ value of complex **2** first decreases slowly and then rapidly, as the temperature is lowered, until reaching a value of 0.69 $cm^3\ mol^{-1}$ K at 2 K (Fig. 5). This behavior implies that antiferromagnetic interactions are present in complex **2**. For complex **1**, $\chi$ and $\chi^{-1}$ experimental values as a function of $T$ were fitted to the Curie–Weiss law (Fig. 6), confirming its purely paramagnetic behavior.

Because of the presence of dinuclear Mn(II) clusters along the 2D polymer structure in **2** (Fig. S3, supplementary data), and considering the plot of $\chi$ versus $T$, where the susceptibility exhibits a maximum at 5.97 K ($T_N$) after which the $\chi$ value starts to decrease, we believed that this compound would present antiferromagnetic interactions within the dimeric Mn(II) unit. Therefore, the experimental data were analyzed using the Bleaney–Bowers Eq. (1) [26] for a coupled $S = 5/2$ dimeric unit.

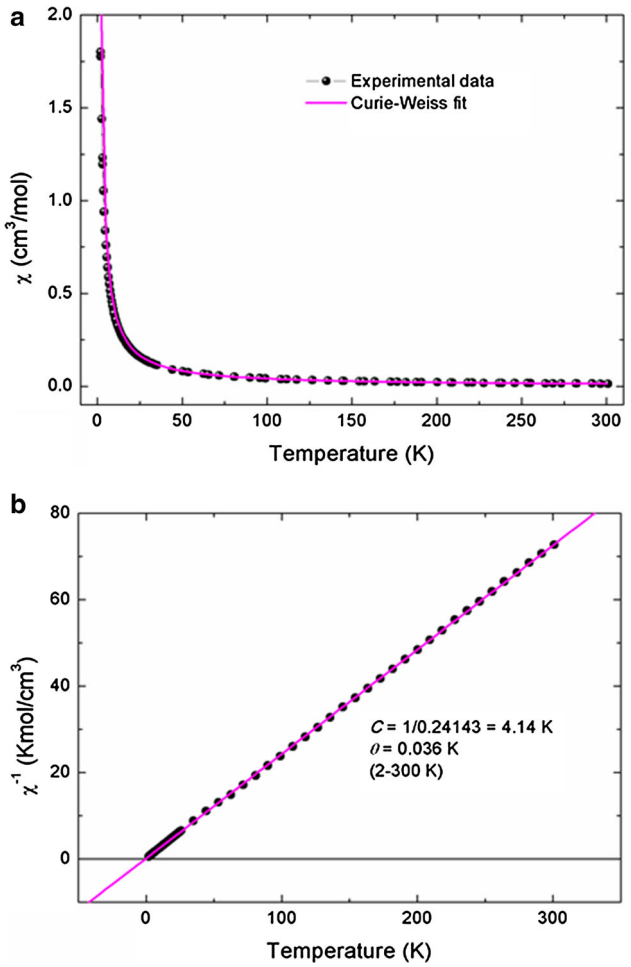


**Fig. 6** $\chi$ versus $T$ plot (**a**) and $\chi^{-1}$ versus $T$ plot (**b**) for **1**

$$\chi = (1-\rho)\frac{N_A g^2 \mu_B^2 \left(2e^{2J/k_B T}\right)}{k_B (T-\theta)(1+3e^{2J/k_B T})} + \rho\frac{N_A g^2 \mu_B^2}{2k_B T} \qquad (1)$$

where $\theta$ is the Curie–Weiss temperature and $J$ is the magnetic spin exchange interaction according to the Hamiltonian interaction: $H = -2\,J\,(S_1 \cdots S_2)$, between two Mn magnetic moments in the dimeric unit. The second term in Eq. (1) refers to the non-interacting paramagnetic species, with the factor $\rho$ as the molar fraction of these paramagnetic moments; $k_B$ is the Boltzmann constant, $N_A$ is the Avogadro number and $\mu_B$ the Bohr magneton. The best fit of the experimental data was obtained with $J/k_B = -3.64$ K, $g = 2.27$, $\theta = -12.8$ K and $\rho = 6.3$ % (Fig. 7a). Thus, the Bleaney–Bowers equation describes very well the experimental results, confirming the antiferromagnetic interaction between paired Mn(II) centers. This model has been applied for coordination polymers having similar dinuclear units to those in complex **2** [27]. Figure 7b shows the result of the fitting with the Curie–Weiss law. The Curie–Weiss plot for **2** gave constants: $C = 9.26$ cm$^3$ K mol$^{-1}$, $\theta = -15.22$ K, thus validating, the weak antiferromagnetic exchange occurring between

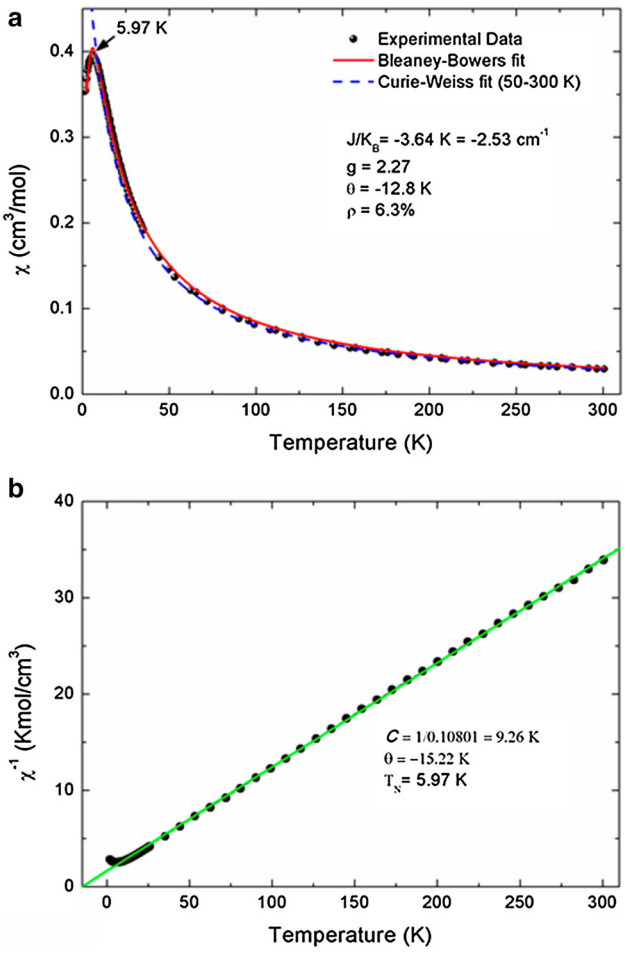


**Fig. 7** $\chi$ versus $T$ plot (**a**) and $\chi^{-1}$ versus $T$ plot (**b**) for **2**

Mn(II) ions in the dinuclear units of **2**. Comparable $J$ values have been obtained for other similar weak antiferromagnetic systems [28]. Overall, the magnetic behavior of **2** agrees very well with a weak antiferromagnetic intramolecular interaction between Mn(II) ions, which has usually been found for the *syn–syn*, equatorial–equatorial arrangement in carboxylate bridged metal centers in analogous dinuclear units [20]. The observed magnetic behaviors are in very good concordance with the Mn···Mn distances found in **1** and **2**. Polymer **2** exhibits the shortest distance between ions (4.561 Å); therefore, it exhibits magnetic interactions. Conversely, magnetic exchange was not found in **1**, where the metal ion distances vary from 7.012 to 9.885 Å.

## Conclusion

We have reported the synthesis and characterization of two Mn coordination polymers with fumarato and two different dimethyl-2,2′-bipyridine co-ligands. In **1**, the bridging fum ligand coordinates as $\eta^1{:}\eta^0$, yielding a 1D polymer; while

in **2**, fum can be found in $\eta^1$:$\eta^1$ and $\mu_2$–$\eta^1$:$\eta^1$ modes, generating a 2D structure. The origin of these dissimilar structures is attributed to the differing steric requirements of the dimethyl-2,2′-bipyridine ancillary ligands. Reduced steric hindrance leads to higher structural dimensionality, as in the 2D polymer **2**. The structural differences of the complexes **1** and **2** are also reflected in their thermal and magnetic properties. Thus, polymer **1** exhibits only a paramagnetic behavior, while the negative values obtained for $J$ and $\theta_{C-W}$ are indicative of intra-dimer Mn(II) weak antiferromagnetic interactions in polymer **2**.

## Supplementary data

CCDC-993491 and 995619 contain supplementary crystallographic data for **1** and **2**, respectively. These data can be obtained free of charge via http://www.ccdc.cam.ac.uk/conts/retrieving/html or from Cambridge Crystallographic Data Center (CCDC), 12 Union Road, Cambridge CB2 1EZ, UK [Fax: (+44) 1223-336-033; Email: deposit@cdc.cam.ac.uk].

**Acknowledgments** Authors are indebted to Dr. Diego Martínez-Otero (CCIQS UAEM-UNAM) and M. en C. Alejandra Nuñez (CCIQS UAEM-UNAM) for single-crystal X-ray diffraction and elemental analyses, respectively. Funding for this work was provided by Universidad Autónoma del Estado de México. This work was also supported by CONACyT project 129293, DGAPA-UNAM project IN106014, and ICYTDF, project PICCO. R.E. thanks to A. López, and A. Pompa-Garcia (IIM-UNAM), for help in computational and technical problems.

## References

1. Robson R (2008) Dalton Trans 5113
2. Dua M, Li C-P, Liub C-S, Fang S-M (2013) Coord Chem Rev 257:1282
3. Das D, Banerjee R, Mondal R, Howard JAK, Boese R, Desiraju GR (2006) Chem Commun 555
4. Desiraju GR, Vittal JJ, Ramanan A (2011) Crystal engineering-a text book. IISc Press and World Scientific, Singapore
5. Zhou XH, Li L, Li HH, Li A, Yang T, Huang W (2013) Dalton Trans 42:12403
6. Curiel D, Más-Montoya M, Sánchez G (2014) Coord Chem Rev 284:19
7. Shi Z, Zhang L, Gao S, Yang G, Hua J, Gao L, Feng S (2000) Inorg Chem 39:1990
8. Bora SJ, Das BK (2012) J Solid State Chem 192:93
9. Téllez-López A, Jaramillo-García J, Martínez-Domínguez R, Morales-Luckie RA, Camacho-López MA, Escudero R, Sánchez-Mendieta V (2015) Polyhedron 100:373
10. Patrick BO, Reiff WM, Sanchez V, Storr A, Thompson RC (2004) Inorg Chem 43:2330
11. Zheng YQ, Lin JL, Chen BY (2003) J Mol Struct 646:151
12. Devereux M, McCann M, Leon V, Geraghty M, McKee V, Wikaira J (2000) Polyhedron 19:1205
13. Hancock RD (2013) Chem Soc Rev 42:1500
14. Alizadeh R, Amani V (2016) Inorg Chim Acta 443:151
15. Lopes LB, Corrêa CC, Guedes GP, Vaz MGF, Diniz R, Machado FC (2013) Polyhedron 50:16
16. Zhang GM, Li Y, Zou XZ, Zhang JA, Gu JZ, Kirillov AM (2016) Transition Met Chem 41:153
17. APEX 2 software suite (2012) Bruker AXS Inc., Madison
18. Sheldrick GM, SHELX (2008) Acta Crystallogr Sect A 64:112
19. Hübschle CB, Sheldrick GM, Dittrich B, ShelXle (2011) Appl Cryst 44:1281
20. Wang CC, Gao F, Guo XX, Jing H-P, Wang P, Gao SJ (2016) Trans Met Chem 41:375
21. Manna SC, Zangrando E, Drew MGB, Ribas J, Chaudhuri NR (2006) Eur J Inorg Chem 481
22. Jin S, Chen W (2007) Inorg Chim Acta 360:3756
23. Gu JZ, Kirillov AM, Wu J, Lv DY, Tang Y, Wu JC (2013) Cryst Eng Comm 15:10287
24. Gu JZ, Gao ZQ, Tang Y (2012) Cryst Growth Des 12:3312
25. Zhao Y, Chang XH, Liu GZ, Ma LF, Wang LY (2015) Cryst Growth Des 15:966
26. Bleaney B, Bowers KD (1952) Proc Roy Soc (London) Ser A 214:451
27. Dey SK, Hazra M, Thompson LK, Patra A (2016) Inorg Chim Acta 443:224
28. Lou Y, Wang J, Tao Y, Chen J, Mishimab A, Ohba M (2014) Dalton Trans 43:8508